School of Mathematics, Meteorology
and Physics

University of

Department of Mathematics

Preprint MPS_2010-21

6 July 2010

Condition Number Estimates for Combined Potential Integral Operators in Acoustics and their Boundary Element Discretisation

by

T. Betcke, S.N. Chandler-Wilde, I.G. Graham,
S. Langdon and M. Lindner

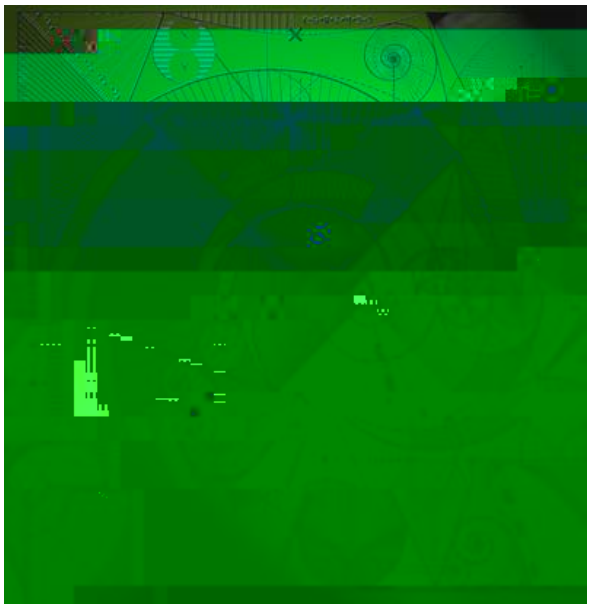

CONDITION NUMBER ESTIMATES FOR COMBINED POTENTIAL INTEGRAL OPERATORS IN ACOUSTICS AND THEIR BOUNDARY ELEMENT DISCRETISATION

T BETCKE[*†**], S N CHANDLER-WILDE[*‡**], I G GRAHAM[§**], S LANGDON[*¶**], AND M LINDNER[‖**]

Abstract. We consider the classical coupled, combined-field integral equation formulations for time-harmonic acoustic scattering by a sound soft bounded obstacle. In recent work, we have proved lower and upper bounds on the L^2 condition numbers for these formulations, and also on the norms of the classical acoustic single- and double-layer potential operators. These bounds to some extent make explicit the dependence of condition numbers on the wave number k, the geometry of the scatterer, and the coupling parameter. For example, with the usual choice of coupling parameter they show that, while the condition number grows like $k^{1=3}$ as $k \to \infty$, when the scatterer is a circle or sphere, it can grow as fast as $k^{7=5}$ for a class of `trapping' obstacles. In this paper we prove further bounds, sharpening and extending our previous results. In particular we show that there exist trapping obstacles for which the condition numbers grow as fast as $\exp(\delta k)$, for some $\delta > 0$, as $k \to \infty$ through some sequence. This result depends on exponential localisation bounds on Laplace eigenfunctions in an ellipse that we prove in the appendix. We also clarify the correct choice of coupling parameter in 2D for low k. In the second part of the paper we focus on the boundary element discretisation of these operators. We discuss the extent to which the bounds on the continuous operators are also satisfied by their discrete counterparts and, via numerical experiments, we provide supporting evidence for some of the theoretical results, both quantitative and asymptotic, indicating further which of the upper and lower bounds may be sharper.

1. Introduction.

Consider scattering of a time-harmonic ($e^{-i\omega t}$ time dependence) acoustic wave u^i by a bounded, sound soft obstacle occupying a compact set $D \subset \mathbb{R}^d$ ($d = 2$ or 3) with Lipschitz boundary Γ, which is such that the complement set $\Omega_e := \mathbb{R}^d \setminus D$ is connected. The medium of propagation, occupying Ω_e, is assumed to be homogeneous, isotropic and at rest. Under the assumption that u^i is an entire solution of the Helmholtz (or reduced wave) equation with *wavenumber* $k = \omega/c > 0$ (where $c > 0$ denotes the speed of sound), we seek the resulting time-harmonic acoustic pressure field u, satisfying the Helmholtz equation

$$\Delta u + k^2 u = 0 \qquad \text{in} \qquad \Omega_e; \tag{1.1}$$

This is to be solved subject to the sound soft boundary condition

$$u = 0 \qquad \text{on} \qquad \Gamma = \partial\Omega_e; \tag{1.2}$$

and the Sommerfeld radiation condition, which requires that

$$\frac{\partial u^s}{\partial r} - iku^s = o(r^{-(d-1)/2}) \tag{1.3}$$

---

[*]Department of Mathematics, University of Reading, Whiteknights, PO Box 220, Berkshire RG6 6AX, UK

[†]Email: t.betcke@reading.ac.uk

[‡]Email: s.n.chandler-wilde@reading.ac.uk

[§]Department of Mathematical Sciences, University of Bath, Bath BA2 7AY, UK. Email: I.G.Graham@bath.ac.uk

[¶]Email: s.langdon@reading.ac.uk

[‖]TU Chemnitz, Fakultät für Mathematik, 09107 Chemnitz, Germany. Email: mali@hrz.tu-chemnitz.de

[**]The authors gratefully acknowledge helpful discussions with Alex Barnett (Dartmouth), Peter Chamberlain (Reading), and Michael Levitin (Reading). Timo Betcke is supported by Engineering and Physical Sciences Research Council (EPSRC) Grant EP/H004009/1, Marko Lindner is partially supported by a Marie Curie Fellowship of the European Commission (MEIF-CT-2005-009758), and the other authors are supported by EPSRC Grant EP/F067798/1.

(Throughout the paper $k \cdot k$ denotes the L^2

detailed k–explicit numerical analysis of *hp* boundary integral methods for general Helmholtz scattering problems in [24]. There it is shown (for example in [24, Corollary 3.18]) that, provided $\|A_{k,k}^{-1}\| \leq Ck^{\gamma}$ with C and γ independent of k, then an *hp* refinement strategy in which p grows logarithmically in k and h decreases like $k^{-1}\log k^{\gamma}$

For the case $d = 3$, when $¡$ is a sphere of unit radius, it is further shown in [15] that, for all su±ciently large k, (2.1) holds (see also [17]) and that, for every $C^0 > 1$,

$$kA^{\,i\,1}_{k;k}k \cdot C^0; \tag{2.4}$$

for all su±ciently large k. A more re¯ned and °exible upper bound on $A_{k;´}$ than (2.1) in the 3D case was recently derived in [5], where it was shown that, for all su±ciently large k,

$$kD_k k \cdot C; \quad kS_k k \cdot Ck^{\,i\,2=3}; \tag{2.5}$$

for some constant C independent of k, and hence

$$kA_{k;´}k \;=\; kI + D_k \;¡\; i´S_k k \;\cdot\; 1 + C^{\;3}\;1 + j´jk^{\,i\,2=3}\;\;: \tag{2.6}$$

The choice $j´j = k$ yields the same estimate as (2.1), whereas the choice $j´j = k^{2=3}$ yields a k ¡ independent bound for $kA_{k;´}k$.

2.2. The case of a starlike obstacle. Consider the case when - is connected, piecewise smooth and starlike, with ¡ Lipschitz and C^2 in a neighbourhood of almost every $x \,2\, ¡$, and

$$\pm_{¡} := \operatorname*{ess\,inf}_{x\,2\,¡} x \¢ ¤(x) > 0$$

bTD[tsies-301.527(bTD[tnected,1.5TD[(TD[(j)]TJ/F1384and)]TJ/F110TD[(¡,)-332(a59.96Tf5.546)-34474(Une)-3011.5er

$x_{¡}$ ¡

to minimise the condition number of $A_{k;\cdot}$ (and see [3, 4] for some further evidence sup-

$R_0 > 0$ (later we will choose R_0 to be some characteristic length scale of ¡). It is

k

for all $k \geq k_0$ *and all* $\gamma \in \mathbb{R}$.

In fact, under the conditions of Theorem 2.3, assuming further that $f^{(N+1)}(0) \neq 0$, we have quantitative lower bounds on $\|S_k\|$ and $\|A_{k;\gamma}\|$:

$$\|S_k\| \geq C_N(0)\, k^{-(N+1)/(2N+1)}\,(1 + o(1)); \quad \text{as } k \to \infty; \tag{2.20}$$

and

$$\|A_{k;\gamma}\| \geq \begin{cases} |\gamma|\, C_N(0)\, k^{-(N+1)/(2N+1)}\,(1 + o(1)); & \text{if } |\gamma| k^{-(N+1)/(2N+1)} \to \infty; \\ |\gamma|\, C_N(0)\, k^{-(N+1)/(2N+1)} - \frac{N}{2^{N/2}} + o(1); & \text{if } |\gamma| = k^{(N+1)/(2N+1)}; \end{cases} \tag{2.21}$$

as $k \to \infty$, where

$$C_N(0) = \left(\frac{1}{8\pi}\right)^{N/2} \left(\frac{N!}{2\,|f^{(N+1)}(0)|}\right)^{1/(2N+1)}.$$

Noting that $f''(0)$ is the curvature at $x^\natural$, we have the following corollary by applying these equations with $N = 1$.

Corollary 2.4. *[10, Corollary 4.5] Suppose (in the 2D case) that* Ω *is locally* C^2 *in a neighbourhood of some point* $x^\natural$ *on the boundary and let* R *be the radius of curvature at* $x^\natural$. *If* $R < \infty$, *then,*

$$\|S_k\| \geq \frac{1}{2}\left(\frac{R}{\pi}\right)^{1/3} (2k)^{-2/3}(1 + o(1)); \quad \text{as } k \to \infty; \tag{2.22}$$

and

$$\|A_{k;\gamma}\| \geq \begin{cases} \left(|\gamma| - \frac{1}{2}\left(\frac{R}{\pi}\right)^{1/3}\right)(2k)^{-2/3}(1 + o(1)); & \text{if } |\gamma| k^{-2/3} \to \infty \end{cases}$$

Then there exist $C > 0$ *and* $k_0 > 0$ *such that*

$$\|D_k\| \leq Ck^{N/(4N+4)}$$

for all $k > k_0$.

2.5. Lower bounds on $\|A_{k;\Gamma}^{i\,1}\|$ for trapping obstacles. In [10] it is shown that if Γ is a certain type of trapping obstacle then $\|A_{k;\Gamma}^{i\,1}\|$ can be unbounded as $k \to \infty$. The type of trapping obstacle considered in [10] is an obstacle for which there exists points P and Q on the boundary $\partial\Omega$ such that:

(i) $\partial\Omega$ is C^1 in neighbourhoods of P and Q;

(ii) the line segment joining P and Q lies in Ω_e and;

(iii) this line segment is normal to $\partial\Omega$ at P and Q.

The line segment PQ is an example of a *periodic orbit*, by which we mean that it is the possible locus of a point billiard particle moving in the exterior region Ω_e in a straight line at unit speed as on an ideal billiard table, interacting with the boundary $\partial\Omega$ according to the usual law of specular reflection (angle of reflection equals angle of incidence).

for m

where Φ_{k_m} denotes the fundamental solution Φ of the Helmholtz equation in 2D in the case $k = k_m$. Then we can view $v_m \in C^2(\bar{\Omega}_e)$ as the total field for the problem of scattering by the obstacle Ω in the case when v_m^i is the incident field. For defining $v_m^s := v_m - v_m^i$ it holds that $\Delta v_m^s + k_m^2 v_m^s = 0$ in Ω_e, that v_m^s satisfies the Sommerfeld radiation condition (since v_m^i does and v_m is compactly supported), and that $v_m^s = -v_m^i$ on Γ. It follows, arguing as in the proof of [10, Theorem 5.1], that

$$A'_{k_m,\eta} \frac{\partial v_m}{\partial \nu} = f_m$$

(cf. (1.9)), where

$$f_m(x) := 2\frac{\partial v_m^i}{\partial \nu}(x) - 2i\eta v_m^i(x), \quad x \in \Gamma. \tag{2.32}$$

Since $\|A'^{-1}_{k_m,\eta}\| = \|(A'_{k_m,\eta})^{-1}\|$, our proof of (2.25) will be completed if we can show that, for some constant $\gamma > 0$,

$$\left\| \frac{\partial v_m}{\partial \nu} \right\|_{L^2(\Gamma)} \le C e^{\gamma k_m} \left(1 + \frac{|\eta|}{k_m} \right)^{-1} \|f_m\|_{L^2(\Gamma)}, \tag{2.33}$$

for $m = 0, 1, \ldots$ and $\eta \in \mathbb{R} \setminus \{0\}$.

To see that (2.30) implies (2.33), we use (2.31), and we also apply Green's representation theorem [13] to v_m to give that

$$v_m(x) = \int_{\Omega_e} \Phi_{k_m}(x,y) g_m(y)\, dy + \int \Phi_{k_m}(x,y) \frac{\partial v_m}{\partial \nu}(y)\, ds(y), \quad x \in \Omega_e. \tag{2.34}$$

Using the bound (e.g. [10]) that $|H_0^{(1)}(t)| \le \sqrt{2/(\pi t)}$, for $t > 0$, which implies that

$|\Phi_k$

ye4 0 TD[()]1D[(L)]TJ/F218F1211.96 Tf 4f 15.49 0 TD[(j)]6Tf 59.96 Tf 15.49 2D[(L
(ye40 TD 96 Tf 9.85 062n6 that))]TJ/F109.96Tf5.540TD[(dy)]TJ/F109.96Tf196T75l3.870TD[(y)]

and (cf. $x2.3$) $©_0(x;y) := (1=2¼)\log(1=jx\ ¡\ yj)$ is the standard fundamental solution of the Laplace equation. Now, from standard mapping properties of Newtonian potentials, it holds that $w_m^{(0)}\ 2\ H^1(E)$, with $kw_m^{(0)}k_H$

as $k \to 0$ in the 3D case, and that the first of these results holds also in the 2D case. In the 2D case the limiting behaviour of S_k is more subtle. We see from (2.16) that

$$\left\| S_k - S_0 + \frac{1}{2\pi} \log(kR_0)\, T \right\| \to 0 \tag{2.41}$$

as $k \to 0$ where T is the finite-rank integral operator defined by

$$T\phi(x) = \int_\Gamma \phi(y)\, ds(y), \quad x \in \Gamma.$$

The following limiting behaviour of $A_{k,\theta}$ is clear from (2.40) and (2.41).

Lemma 2.9. *As $k \to 0$,*

$$A_{k,\theta} = I + D_0 - i\theta S_0 (1 + o(1)) \tag{2.42}$$

in 3D, while

$$A_{k,\theta} = I + D_0 + i\theta \frac{1}{2\pi} \log(kR_0)\, T - i\theta S_0 (1 + o(1)) \tag{2.43}$$

in 2D. Thus, unless

$$\theta = \begin{cases} O(1); & d = 3; \\ O((\log k)^{-1}); & d = 2; \end{cases} \quad \text{as } k \to 0; \tag{2.44}$$

it holds that $\|A_{k,\theta}\| \to 1$ as $k \to 0$. On the other hand, if, for some $c_0 \in \mathbb{R}$,

$$\theta \to c_0 \quad \text{as } k \to 0; \tag{2.45}$$

is well known that A_0 is not injective, having a non-trivial null space which is the set of constant functions, see e.g. [22, Theorem 6.20], [31]. To show invertibility of A_0 for $c_0 \neq 0$ we note first that, by interpolation, it is enough to show invertibility on $H^s(\Gamma)$ for $s = 0$ and 1 [26]. Further, since the difference $A_0 - A_{k,\eta}$ is a compact operator on $L^2(\Gamma)$ and on $H^1(\Gamma)$ (see e.g. the proof of Theorem 2.7 in [9]) and since $A_{k,\eta}$ is invertible, it holds that A_0 is Fredholm of index zero on $L^2(\Gamma)$ and on $H^1(\Gamma)$, so that it is invertible if and only if it is injective. Moreover, since A_0 is Fredholm with the same index on $H^1(\Gamma)$ and $L^2(\Gamma)$, and $L^2(\Gamma)$ is dense in $H^1(\Gamma)$, it follows from a standard result on Fredholm operators (see e.g. [28, *x*1]), that the null-space of A_0 is a subset of $H^1(\Gamma) \subset H^{1/2}(\Gamma)$. In the case that Γ is C^2 that there are no non-trivial functions in the null-space of A_0 in $C(\Gamma)$ is shown in [22, Theorem 6.24] in the case $d = 2$ and in [12, Theorem 3.33] in the case $d = 3$. In the case when Γ is Lipschitz the same arguments can be used to prove injectivity of A_0 in $H^{1/2}(\Gamma)$, replacing the mapping properties of layer potentials in classical function spaces in [12, 22] with those in Sobolev spaces in [26] (cf. the proof of Theorem 2.5 in [9]). □

2.7. Bounds on condition numbers and choice of η. In this section we bring together the results from the sections above and explore their implications for the conditioning of $A_{k,\eta}$, and what this then implies regarding the choice of η to minimise cond $A_{k,\eta}$. We have already noted in *x*2.2 and *x*2.6 recommendations made in the literature regarding the choice of η, mainly based on study of the case when Γ is a circle or sphere. Overwhelmingly (see e.g. [20, 21, 3, 4, 17, 7, 8, 15]) the guidance is to take η proportional to k for all but small values of k. The choice of η for small k has been discussed already in *x*2.6. One choice of η, recommended by Kress [20] for the 3D case, that we have studied in *x*2.2, is $\eta = \max(1/(2R_0); k)$. This choice, by Lemma 2.9 above, is not suitable in the 2D case for low k, since with this choice $\|A_{k,\eta}\| \to 1$ as $k \to$ /F109.96Tf4.471.49TD[())]TJ/F139.96Tf3.870TD[(;)-166(k39.96Tf(1)]TJ/F109.06[(=)-359(49.9

3. Discrete level. In this section we explore the relationship between $kA_{k;\cdot}k$ and $kA_{k;\cdot}^{-1}k$ and the norms of discrete versions of these operators, specifically the norms of matrices arising from Galerkin discretisations.

Let $X_N \subset L^2(\Omega)$ be a finite-dimensional subspace with $P_N : L^2(\Omega) \to X_N$ the corresponding orthogonal projection. Let V be a bounded linear operator on $L^2(\Omega)$. Then, given $y \in L^2(\Omega)$, a Galerkin method for solving the equation

$$Vx = y$$

for $x \in L^2(\Omega)$, is to seek $x_N \in X_N$ such that

$$P_N V x_N = P_N y. \tag{3.1}$$

Let $\{\phi_1, \ldots, \phi_N\}$ be an orthonormal basis of X_N, define $V_N : X_N \to X_N$ by $V_N := P_N V|_{X_N}$, and let $T_N : X_N \to \mathbb{C}^N$ be defined by

$$T_N x = [(x, \phi_1), \ldots, (x, \phi_N)]^T.$$

Then T_N is an isomorphism, indeed an isometric isomorphism if we give $\mathbb{C}^N$ the standard Euclidean norm $\|\cdot\|_2$. Further (3.1) is equivalent to

$$V^N T_N x_N = T_N P_N y,$$

where

$$V^N := T_N V_N T_N^{-1}$$

is the linear operator on $\mathbb{C}^N$ whose matrix representation (that we denote also by V^N) is the Galerkin matrix $V^N = [(V\phi_j, \phi_i)]$. Clearly

$$\|V_N\| = \|V^N\| \tag{3.2}$$

(where we use $\|\cdot\|$ on the right hand side to denote the matrix norm induced by the vector norm $\|\cdot\|_2$), since both T_N and T_N^{-1} are isometries. Also V_N is invertible if and only if V^N is invertible and, if they are both invertible, then

$$\|V_N^{-1}\| = \|(V^N)^{-1}\|.$$

Now we need to determine the relationship between $\|V_N\|$ and $\|V\|$. We first require the following result.

Lemma 3.1. *If W is a bounded linear operator on $L^2(\Omega)$ and $P_1, P_2, \ldots$ is a sequence of orthogonal projection operators with $P_N\phi \to \phi$ for all $\phi \in L^2(\Omega)$, then*

$$\|P_N W P_N\| \to \|W\|,$$

as $N \to \infty$.

Proof. Let $\gamma = \liminf_{N\to\infty} \|P_N W P_N\|$ and choose a monotonic increasing sequence $N_1, N_2, \ldots$ of natural numbers with $\|P_N$

$C^{(j)}$

4. Numerical results. In this section we compute $\|V^N\|$ for $V = S_k; D_k; A_{k;\acute{}}$, and $\|(V^N)^{i\,1}\|$ for $V = A_{k;\acute{}}$, each for a variety of obstacles, and we compare the computed values with the upper and lower bounds on the corresponding continuous operators as described in *x*2. The aim is to provide supporting evidence for some of the theoretical results described in *x*2, both quantitative and asymptotic, and to give some indication of which of the upper and lower bounds may be sharper, particularly when there is a signi¯cant gap between them. We also seek an indication of the extent to which the bounds on the continuous operators are satis¯ed by their discrete counterparts.

We present results for $\acute{} = k$ for all geometries under consideration, and we also present results for $\acute{} = k^{2=3}$ for certain speci¯c examples. As we have discussed in *x*2.7, the choice $\acute{} = k$ is widespread in the literature, e.g. [3, 4, 15, 17, 20], and this choice is supported by our own preceding analysis. The interesting choice $\acute{} = k^{2=3}$, proposed in [5], is also supported by some of the above analysis; for example we have seen in *x*2.7 that, for a circular scatterer, cond $A_{k;\acute{}}$ increases at the same rate as $k \to 1$ whether $\acute{}$ is proportional to k or proportional to $k^{2=3}$.

Although our main focus is on larger values of k, for two examples we also investigate the limit $k \to 0$, presenting results for $\acute{} = k$ and for $\acute{}$ given by (2.49).

In each example the boundary ¡ is piecewise C^1, that is $¡ = \sum_{j=1}^{p} ¡^{(j)}$ with $¡^{(j)}$ a C^1 arc. We denote the length of $¡^{(j)}$ by L_j, and divide each $¡^{(j)}$ into N_j segments $¡_i^{(j)}$, $i = 1;\ldots;N$ (!

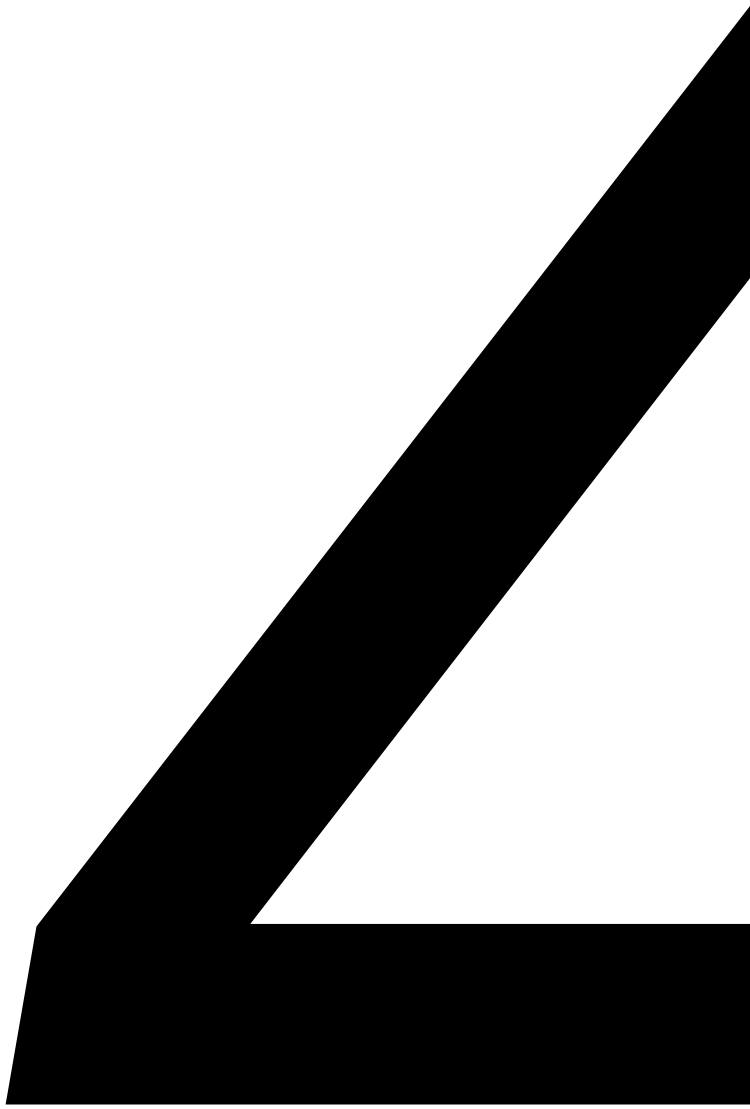

Fig. 4.1. *Obstacles corresponding to numerical experiments.*

where here and throughout this section $o(1)$ denotes a term which vanishes in the limit as $k \to 1$. Theorem 2.6, (2.3) and (2.12) imply that, for $k > 0$,

$$C_1 \cdot \|D_k\| \cdot C_2 k^{1=2} + C_3;$$

whilst we know that the sharper upper bound (2.5) holds in the case of a sphere, that $\|D_k\| \cdot C$. The numerical results in Table 4.1 for the corresponding boundary element matrices suggest that this sharper result, proved for a sphere, appears to be applicable for a circle as well; we observe for the discrete approximations that $\|S_k\| \gg k^{i\,2=3}$ and $\|D_k\| \gg k^0$ ($\gg$ in this section indicates that the ratio of the left hand side to the right hand side is approximately constant in the limit $k \to 1$). The quantitative lower bound on k=e(0-222.0 TD[(])]TJ/F4 1.eee ().6 (the)-435(ca 41 4-31 2560o[(C)]TJ/F4 6.97 Tf

k	$(32\pi)^{-1/3}k^{-2/3}$	$\|S_k\|$	p	$\|D_k\|$
5	7.355×10^{-2}	5.240×10^{-1}		1.144
10	4.633×10^{-2}	3.152×10^{-1}	-0.73	1.114
20	2.919×10^{-2}	1.997×10^{-1}	-0.66	1.084
40	1.839×10^{-2}	1.246×10^{-1}	-0.68	1.079
80	1.158×10^{-2}	7.798×10^{-2}	-0.68	1.076
160	7.297×10^{-3}	4.884×10^{-2}	-0.68	1.075
320	4.597×10^{-3}	3.076×10^{-2}	-0.67	1.072
640	2.896×10^{-3}	1.935×10^{-2}	-0.67	1.071

Table 4.1

Circle. *Norms of Galerkin BEM approximations to S_k and D_k, and p values given by* (4.1).

from Lemma 2.1. The upper bound on $\|A_{k;k^{2/3}}\|$ for the case of a sphere is, from (2.6), $\|A_{k;k^{2/3}}\| \cdot C_3$. The numerical results in Table 4.2 suggest that this sharper result also holds for a circle; the results suggest $\|A_{k;k^{2/3}}\| \gg k^0$, and that $\|A_{k;k}\| \gg k^{1/3}$ as expected. The quantitative lower bound on $\|A_{k;k}\|$ from Corollary 2.4 is a lower bound in Table 4.2, underestimating the true norm by a factor of about 7.

k	$\left(\frac{k}{32\pi}\right)^{1/3}$	$\|A_{k;k}\|$	p	$\|A_{k;k}^{-1}\|$	$\|A_{k;k^{2/3}}\|$	$\|A_{k;k^{2/3}}^{-1}\|$	p	$B_{0;k^{2/3}}$
5	0.37	2.663		0.986	2.016	0.995		3.82
10	0.46	3.233	0.28	0.987	1.993	1.056	0.09	4.49
20	0.58	4.021	0.32	0.987	1.981	1.260	0.26	5.38
40	0.74	5.030	0.32	0.987	2.000	1.701	0.43	6.56
80	0.93	6.271	0.32	0.987	1.999	2.039	0.26	8.06
160	1.17	7.859	0.33	0.987	1.990	2.694	0.40	9.98
320	1.47	9.883	0.33	0.987	1.998	3.407	0.34	12.40
640	1.85	12.419	0.33	0.987	2.000	4.307	0.34	15.49

Table 4.2

Circle. *Galerkin BEM approximations to $\|A_{k;\eta}\|$ and $\|A_{k;\eta}^{-1}\|$.*

By Lemma 2.1, $\|A_{k;k}^{-1}\| \geq 1$, which combined with (2.2) implies that $\|A_{k;k}^{-1}\| = 1$ for all k sufficiently large, and the numerical results in Table 4.2 show this behaviour. The bound for general starlike obstacles applied to the circle, i.e. (2.8), gives that

$$\|A_{k;\eta}^{-1}\| \cdot \frac{1}{2} + \left(1 + \frac{k^2}{\eta^2} + \frac{(1+2k)^2}{2\eta^2}\right)^{1/2} =: B_{0;\eta}.$$

Note that $B_{0;k} > 2.5$ (in fact it holds that $2.5 \cdot B_{0;k} \cdot 2.6$ for the range of k in Table 4.2), and that $B_{0;k^{2/3}} \gg \sqrt{3}k^{1/3}$ as $k \to \infty$. We see from Table 4.2 that $B_{0;\eta}$ appears to be an upper bound for the discretisation of $\|A_{k;\eta}^{-1}\|$ as predicted, overestimatimating by a factor of about 2.5 for the larger values of k when $\eta = k$, by a factor of about 3.6 when $\eta = k^{2/3}$.

We note from Table 4.2 that, for this example, the condition number $\text{cond}\, A_{k;\eta} = \|A_{k;\eta}\|\|A_{k;\eta}^{-1}\|$ appears to be slightly numerically smaller for $\eta = k^{2/3}$ than for $\eta = k$. It appears that, for both choices of η, $\text{cond}\, A_{k;\eta}$ increases approximately in proportion to $k^{1/3}$, though this is less clear in the case $\eta = k^{2/3}$.

4.2. Ellipse. Next we consider the ellipse given by $(2\cos t; \frac{1}{2}\sin t)$, $t \in [0; 2\pi]$. The more specific results of §2.1 do not apply in this case, and for upper bounds

on $kS_k k$ and $kD_k k$ we have only the results for general Lipschitz ¡ of x2.3. The inequalities (2.22) and (2.11) imply that, for k ¸ 1,

$$(4¼)^{i\,1=3} k^{i\,2=3}(1 + o(1)) \cdot kS_k k \cdot Ck^{i\,1=2};$$

the lower bound larger than for the case of the circle as the maximum radius of curvature (R = 8) is larger. Theorem 2.6 and (2.12) with N = 0 imply that, for $k > 0$,

$$C_1 \cdot kD_k k \cdot C_2 k^{1=2} + C_3:$$

Inspecting the numerical results in Table 4.3, we see that the quantitative lower bound on $kS_k k$ from (2.22) is clearly a lower bound for the norm of the discretised operator, underestimating the true norm by a factor of about 6 at the highest wavenumbers (cf. the results for the circle). The numerical results for $kD_k k$ suggest that $kD_k k$ » k^0, i.e. that the lower bound on $kD_k k$ is sharp, while it appears from the numerical results that $kS_k k$ » k^p, for p ¼ ¡0:6.

k	$(4¼)^{i\,1=3} k^{i\,2=3}$	$kS_k k$	p	$kD_k k$	p
5	1.471£10$^{i\,1}$	6.692£10$^{i\,1}$		1.458	
10	9.267£10$^{i\,2}$	4.143£10$^{i\,1}$	-0.69	1.591	0.13
20	5.838£10$^{i\,2}$	2.730£10$^{i\,1}$	-0.60	1.671	0.07
40	3.678£10$^{i\,2}$	1.803£10$^{i\,1}$	-0.60	1.760	0.08
80	2.317£10$^{i\,2}$	1.209£10$^{i\,1}$	-0.58	1.819	0.05
160	1.459£10$^{i\,2}$	8.029£10$^{i\,2}$	-0.59	1.877	0.05
320	9.194£10$^{i\,3}$	5.269£10$^{i\,2}$	-0.61	1.919	0.03
640	5.792£10$^{i\,3}$	3.427£10$^{i\,2}$	-0.62	1.942	0.02

Table 4.3

Ellipse. *Galerkin BEM approximations to $kS_k k$ and $kD_k k$.*

k	$\left(\frac{k}{4¼}\right)^{1=3}$	$kA_{k;k}k$	p	$kA^{i\ 1}_{k;k}k$	$kA_{k;k^{2=3}}k$	$kA^{i\ 1}_{k;k^{2=3}}k$	p
5	0.736	3.507		0.987	2.417	0.996	
10	0.927	4.267	0.28	0.987	2.473	1.024	0.04
20	1.168	5.589	0.39	0.987	2.554	1.300	0.34
40	1.471	7.317	0.39	0.987	2.599	1.662	0.35
80	1.853	9.751	0.41	0.987	2.580	1.986	0.26

ables andF-252/-6,variousF204.1395.872130

x^2 (see Figure 4.2), and recalling (2.12), we have, for $k \gg 1$,

$$C_1 k^{1=6} \cdot kD_k k \cdot C_2 k^{1=2}:$$

The numerical results in Tables 4.5 and 4.6 provide some support for these estimates. The lower bound on $kS_k k$ seems sharper than the upper bound, although in fact the behaviour of $kS_k k$ appears to be rather similar to that for the ellipse. On the other hand, the behaviour of *kTf15.490TD[(D)]TJ0ur of*

The results in Table 4.7 clearly demonstrate that $kS_k k \gg k^{-1=2}$ (cf. [32]), a slower rate of decay than for the circle, ellipse or kite, and that the values of $kS_k k$ are bracketed between the quantitative upper and lower bounds in (4.5), nearly coinciding with the lower bound values.

k	$kS_k k$	p	$\sqrt{1=(¼k)}$	$2\sqrt{1=(¼k)}$
5	$2.649£10^{-1}$		$2.523£10^{-1}$	$5.046£10^{-1}$
10	$1.817£10^{-1}$	-0.54	$1.784£10^{-1}$	$3.568£10^{-1}$
20	$1.266£10^{-1}$	-0.52	$1.262£10^{-1}$	$2.523£10^{-1}$
40	$8.960£10^{-2}$	-0.50	$8.921£10^{-2}$	$1.784£10^{-1}$
80	$6.326£10^{-2}$	-0.52	$6.308£10^{-2}$	$1.262£10^{-1}$
160	$4.472£10^{-2}$	-0.50	$4.460£10^{-2}$	$8.921£10^{-2}$
320	$3.162£10^{-2}$	-0.50	$3.154£10^{-2}$	$6.308£10^{-2}$
640	$2.236£10^{-2}$	-0.50	$2.230£10^{-2}$	$4.460£10^{-2}$

Table 4.7

Crack. *Galerkin BEM approximations for $kS_k k$, and theoretical lower and upper bounds.*

4.5. Square. Computed estimates for $kS_k k$, $kD_k k$, $kA_{k;k} k$, $kA^{-1}_{k;k} k$, $kA_{k;k^{2=3}} k$ and $kA^{-1}_{k;k^{2=3}} k$ for the square of side length two are shown in Tables 4.8 and 4.9 below, for various k. The theoretical upper bounds from $x2$ that apply are identical to those for the ellipse and kite examples above. In particular, since the square is starlike satisfying the conditions of $x2.2$, the bounds (4.4) apply. However, as ¡ now contains a straight line segment we have di®erent lower bounds on $kS_k k$, $kA_{k;\cdot} k$ and $kD_k k$ compared to the ellipse and the kite. Speci¯cally, applying Theorem 2.2 and recalling (2.11) and (2.13), it follows that, for $k \gg 1$,

$$\sqrt{\frac{2}{¼k}} + O(k^{-1}) \quad \cdot kS_k k \cdot \quad Ck^{-1=2}; \tag{4.6}$$

$$\sqrt{\frac{2k}{¼}} - 1 + O(1) \quad \cdot kA_{k;k} k \cdot \quad Ck^{1=2}; \tag{4.7}$$

$$\sqrt{\frac{2}{¼}} k^{1=6} - 1 + O(k^{-1=3}) \cdot kA_{k;k^{2=3}} k \cdot Ck^{1=2}. \tag{4.8}$$

Applying Theorem 2.5 and recalling (2.12), we also have

$$C_1 k^{1=4} \cdot kD_k k \cdot C_2 k^{1=2}. \tag{4.9}$$

It appears from Table 4.8 that $kS_k k \gg k^{-1=2}$, as expected, and the quantitative lower bound in (4.6) appears to be sharp, underestimating $kS_k k$ by only 3% at the highest frequency. It also seems that $kD_k k \gg k^{1=4}$, indicating that the lower bound in (4.9) is sharp in its dependence on k.

The results in Table 4.9 suggest that $kA_{k;k} k \gg k^p$, with $p ¼ 1=2$, as expected from (4.7). It appears that $kA_{k;k^{2=3}} k$ is increasing roughly like $k^{1=5}$. The quantitative lower bound in (4.8) is seen to be a lower bound for the Galerkin BEM discretisation of $kA_{k;k^{2=3}} k$ in Table 4.9, underestimating $kA_{k;k^{2=3}} k$ by about a factor 3.5 at the highest frequency. As in the cases of the circle, ellipse, and kite, $kA^{-1}_{k;k} k ¼ 1$ for all k, while $kA^{-1}_{k;k^{2=3}} k$ is increasing as k increases, though the rate of increase is somewhat erratic (from (2.7), we recall that $kA^{-1}_{k;k^{2=3}} k \cdot Ck^{1=3}$). However, it appears that

k	$\sqrt{\frac{2}{\pi k}}$	$\|S_k\|$	p	$\|D_k\|$	p
5	3.568×10^{-1}	5.784×10^{-1}		1.316	
10	2.523×10^{-1}	3.353×10^{-1}	-0.79	1.488	0.18
20	1.784×10^{-1}	2.137×10^{-1}	-0.65	1.730	0.22
40	1.262×10^{-1}	1.428×10^{-1}	-0.58	2.018	0.22
80	8.921×10^{-2}	9.760×10^{-2}	-0.55	2.389	0.24
160	6.308×10^{-2}	6.723×10^{-2}	-0.54	2.825	0.24
320	4.460×10^{-2}	4.667×10^{-2}	-0.53	3.346	0.25
640	3.154×10^{-2}	3.259×10^{-2}	-0.52	3.972	0.25

Table 4.8

Square. *Galerkin BEM approximations for $\|S_k\|$ and $\|D_k\|$.*

cond $A_{k;k^{2=3}} \approx k^p$, with $p = 0.6$, a faster rate of growth than cond $A_{k;k} \approx k^{1=2}$, and, for the largest value of k, cond $A_{k;k} =$ cond $A_{k;k^{2=3}}$.

Where $R_0 > 0$ is some length scale of the scatterer, it follows from Theorem 2.11 that choosing

$$\gamma = \gamma_\star := 1/(R_0(1 - \ln(kR_0)));$$

ensures $\|A_{k;\gamma}\|$ and $\|A_{k;\gamma}^{-1}\|$ remain bounded as $k \to 0$. This is true for any Lipschitz β and (rather arbitrarily) we choose this example to illustrate this numerically. Define R_0 as in §2.2, so $R_0 = \sqrt{2}$ for this particular scatterer (taking the origin at the centre of the square). With this choice of R_0, we show in Table 4.10 norm computations for small values of k. We see that, while $\|A_{k;k}^{-1}\|$ seems to blow up for small values of k, the values of $\|A_{k;\gamma_\star}^{-1}\|$ remain essentially constant, and cond $A_{k;\gamma_\star}$ appears to be approaching a limit of about 3.7 as $k \to 0$. k4qF126.J/Fbro2f39.9pfor β

k	$\|A_{k;k}\|$	$\|A_{k;k}^{-1}\|$	p	$\|A_{k;\eta^*}\|$	$\|A_{k;\eta^*}^{-1}\|$
10^{-5}	1.608	3684.85		1.738	2.106
10^{-4}	1.608	465.66	-0.89	1.723	2.105
10^{-3}	1.608	61.63	-0.88	1.703	2.104
10^{-2}	1.608	9.04	-0.83	1.680	2.100
10^{-1}	1.612	2.11	-0.63	1.693	2.081
1	2.391	1.88	-0.05	2.534	1.871

Table 4.10

Square. *Galerkin BEM approximations for $\|A_{k;k}\|$, $\|A_{k;k}^{-1}\|$, $\|A_{k;\eta^*}\|$, and $\|A_{k;\eta^*}^{-1}\|$.*

$D_k \subset \mathbb{C}\backslash S_k$ and $x_\S \in \Gamma$ are adjacent points on opposite sides of a thin part of Γ, then $\cdot(x_+;y) \approx \cdot(x_-;y)$, $y \in \Gamma$, so that the integral operator should be badly conditioned. To explore the extent to which this is a problem, and the extent to which the bound (2.7) reflects actual behaviour in this limit, we show estimates for $\|A_{k;k}\|$ and $\|A_{k;k}^{-1}\|$ for a rectangle with side lengths 2 and 0.02 in Table 4.11 below, for various small values of k.

Using the notation of §2.2, for this example we have $\pm^\¤ = \pm^+ = 2$, $\pm_- = 0.02$, and $R_0 = \sqrt{4.0004}$, and (2.7) tells us that

$$\|A_{k;\eta}^{-1}\| \cdot B;$$

where B is as defined in §2.2. However, we see from Table 4.11 that this bound is a gross overestimate, at least provided we choose η carefully. For the definition of B implies that, whatever the choice of $\eta \in \mathbb{R}\backslash\{0\}$,

$$B > \frac{1}{2} + \left(\frac{\pm_+}{\pm_-} + \frac{4\pm^{\¤2}}{\pm_-^2}\right)\left(\frac{\pm_+}{\pm_-} + \frac{\pm^{\¤2}}{\pm_-^2}\right)^{1=2} > 2\frac{\pm^{\¤2}}{\pm_-^2} = 2 \cdot 10^4$$

for this geometry. If we choose $\eta = k$ for small k then, indeed, we see significant blowup as $k \to 0$, as for the case of the square (indeed the values of $\|A_{k;\eta}^{-1}\|$ are similar). But, if we choose $\eta = \eta^\¤ := 1=R_0(1 - \ln(kR_0))$, we know from Theorem 2.11 that $\|A_{k;\eta}^{-1}\|$ must stay bounded as $k \to 0$. In fact we see some mild, logarithmic growth in Table 4.11, but $\|A_{k;\eta^*}^{-1}\|$ is never larger than 26 for the range of k shown.

For the computations in Table 4.11 we used 100 elements on each boundary segment. Comparing the algebraic rates p associated with $\|A_{k;k}^{-1}\|$ for the first three wavenumbers $k = 10^{-5}; 10^{-4}; 10^{-3}$ it appears possible that the discretisation does not fully resolve $\|A_{k;k}^{-1}\|$ for $k = 10^{-5}$ and that the exact value may be higher. However, due to convergence issues of the underlying singular value decomposition for the norm computation no finer discretisation could be used here.

4.7. Rectangular cavity. In the last two numerical examples we explore trapping domains, as studied theoretically in §2.5. The rectangular cavity in Figure 4.1 is defined by the polygon with the following coordinates: $p_0 = 0$, $p_1 = (-c; 0)$, $p_2 = (-c; -\`)$, $p_3 = (\`; -\`)$, $p_4 = (\`; 2c - \`)$, $p_5 = (-c; 2c - \`)$, $p_6 = (-c; 2a)$, $p_7 = (0; 2a)$. Here, $a = 1/4=10$, $c = 1$, and $\` = c - a$. The width of the cavity is $2a = 1/4=5$. Hence we expect resonance values in the negative half of the complex plane close to $k = 5m$, $n \in \mathbb{N}$ (see [6, Figure 5.12] for numerical computations of exterior resonances for this cavity). Since for $k = 5m$ the width of the cavity is an integer multiple of half a wavelength, Theorem 2.7 applies and implies that, for $k = 5m$ and

k	$\|A_{k;k}\|$	$\|A_{k;k}^{i-1}\|$	p	$\|A_{k;\Gamma_*}\|$	$\|A_{k;\Gamma_*}^{i-1}\|$	p
10^{-5}	1.978	3087.76		1.978	25.165	
10^{-4}	1.978	924.25	-0.53	1.978	21.533	-0.07
10^{-3}	1.978	128.19	-0.86	1.978	17.581	-0.09
10^{-2}	1.978	45.28	-0.45	1.978	14.078	-0.10
10^{-1}	1.978	14.43	-0.50	1.978	10.384	-0.13
1	2.050	4.53	-0.50	3.310	3.570	-0.46

Table 4.11

Rectangle of side lengths 2 and 0.02. *Galerkin BEM approximations to $\|A_{k;k}\|$, $\|A_{k;k}^{-1}\|$,*

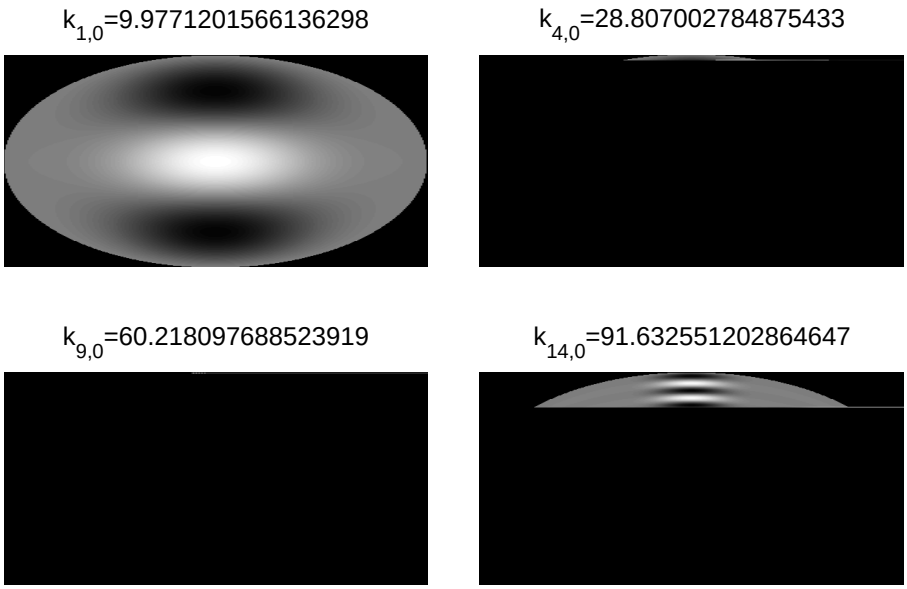

Fig. 4.3. *Some exponentially localised modes of the ellipse associated with zeros of the radial Mathieu function of order* 0. *In the notation of the appendix, the modes plotted are* $u_{m;0}$ *for* $m = 1; 4; 9;$ *and 14, corresponding to the wavenumbers* $k_{m;0}$, $m = 1; 4; 9; 14$.

Estimates for $kA_{k;k}k$ and $kA^{i\,1}_{k;k}k$ for the four wavenumbers from Figure 4.3 are shown in Table 4.13. We expect, from Theorems 2.8 and 2.13, exponential growth of $kA^{i\,1}_{k;k}k$ and cond $A_{k;k}$

5. Conclusions. In this paper we have, in $x2$, summarised what is known regarding upper and lower bounds on the norms of the acoustic single- and double-layer potential operators, S_k and D_k, and the combined layer potential operator $A_{k;\acute{}}$, with an emphasis on how these bounds behave as a function of frequency, and the in°uence of the shape of the boundary. We have also proved sharper upper bounds on kS_kk and $kA_{k;\acute{}}k$ for low k, have summarised what upper and lower bounds on $kA_{k;\acute{}}^{i\ 1}k$ are known, and have shown that exponential growth of $kA_{k;\acute{}}^{i\ 1}k$ is possible as $k\ !\ 1$ through some sequence of wave numbers, in the case of a certain class of 2D trapping obstacles. Finally, we have discussed the condition number cond $A_{k;\acute{}}$, proving that it remains bounded as $k\ !\ 0$ with appropriate choices of the coupling parameter $\acute{}$, and showing that, while it increases as $k\ !\ 1$ only as fast as $k^{1=3}$ for a circle or sphere, and at the rate $k^{1=2}$ for a starlike polygon, it grows exponentially, as k increases through some sequence, for certain trapping obstacles.

In $x3$ we have explored the implications of these results for Galerkin BEM discretisations of these operators, showing that the norms of the Galerkin BEM matrices converge to the norms of the operators that they discretise, as the mesh is re¯ned, and provided an orthonormal basis is used. Convergence to $kA_{k;\acute{}}^{i\ 1}k$ of the norm of the inverse of the matrix corresponding to $A_{k;\acute{}}$ has also been proved in the case that ¡ is C^1. Thus we expect that the norm bounds at the continuous level in $x2$ will apply also at the discrete level if the mesh is su±ciently re¯ned.

This has been con¯rmed in $x4$ where we have explored a range of numerical examples, includes shapes that are convex (both smooth and non-smooth), non-convex but starlike, and non-starlike trapping obstacles. The quantitative upper and lower bounds stated in $x2$ are found to be upper and lower bounds also at the discrete level, and to be rather sharp in many of thew4examples. In T494(has)3y ofhidsshydcone toex3S8(ect)-386TD[(rate)-346(of)

for some $k > 0$.

Let $a = \sqrt{a_1^2 - a_2^2} = a_1\varepsilon$, where $\varepsilon = \sqrt{1 - a_2^2/a_1^2}$ is the eccentricity of the ellipse, and introduce elliptical coordinates (ξ, η), defined by

$$x_1 = a\cosh\xi\cos\eta \quad \text{and} \quad x_2 = a\sinh\xi\sin\eta,$$

in terms of which

$$E = f(a\cosh\xi\cos\eta, a\sinh\xi\sin\eta) : 0 \le \xi \le \xi_0, \ 0 \le \eta < 2\pi\},$$

where $\xi_0 := \tanh^{-1}(a_2/a_1)$. It is well known (see e.g. [35]) that the Laplace operator separates in elliptical coordinates, and that in this coordinate system the Helmholtz equation can be written as

$$\left(\frac{\partial^2}{\partial\xi^2} + \frac{\partial^2}{\partial\eta^2} + k^2a^2(\sinh^2\xi + \sin^2\eta)\right) u = 0. \tag{A.2}$$

Seeking separation of variables solutions in the form $u(x) = M(\xi)N(\eta)$, we see that (A.2) implies that N satisfies the circumferential (or standard) Mathieu equation

$$N''(\eta) + (\lambda - 2q\cos 2\eta)N(\eta) = 0, \tag{A.3}$$

while M satisfies the radial (or modified) Mathieu equation

$$M''(\xi) - (\lambda - 2q\cosh 2\xi)M(\xi) = 0. \tag{A.4}$$

In these equations

$$q = \frac{1}{4}(ka)^2 = \frac{1}{4}(ka_1)^2(1 - (a_2/a_1)^2)$$

and λ is a separation constant. The solutions to (A.3) tJ/F12f139.96Tf19.920TD[(®)]TJ/F149.96Tf8.620TD[(Me)-25r2f13

and only if $M \in C^2(\mathrm{R})$ is an even function that satisfies (A.4). This uniquely specifies M to within multiplication by a constant. The standard notation for this (real-valued) solution is $M(\vartheta) = \mathrm{Mc}_n^{(1)}(\vartheta; q)$; see [14, *x*28.20(iv)] for the standard normalization. Thus we see that $u(x) = M(\vartheta)N(\varphi) = \mathrm{Mc}_n^{(1)}(\vartheta; q)\mathrm{ce}_n(\varphi; q)$ satisfies the full eigenvalue problem (A.1) if and only if

$$\mathrm{Mc}_n^{(1)}(\vartheta_0; q) = 0. \tag{A.6}$$

The complication in computing eigenmodes of the ellipse (for methods see [35, 29]) is that it is a multi-parameter spectral problem: to satisfy (A.6) we have to find a pair $(\mathcal{R}; q)$ such that, simultaneously, (A.3) has a periodic solution and (A.4) has a solution which is even if N is even and which vanishes at ϑ_0. Neves [29] gives a proof based on multi-parameter spectral theory that for each pair $(m; n) \in \{0; 1; \ldots\}^2$ there exists a unique $q_{m;n} > 0$ such that (A.6) holds with $\mathrm{Mc}_n^{(1)}(\mathcal{C}; q_{m;n})$ having m zeros in $(0; \vartheta_0)$. The function

$$u(x) = u_{m;n}(x) := \mathrm{Mc}_n^{(1)}(\vartheta; q_{m;n})\mathrm{ce}_n(\varphi; q_{m;n}) \tag{A.7}$$

is then an eigenfunction of (A.1) for $k = k_{m;n} := \sqrt{4q_{m;n}}/a$. It is well known (e.g. [12]) that the eigenvalues of the Laplace operator have infinity as the only accumulation point, so that $k_{m;n} \to \infty$ as $m + n \to \infty$.

For some $\varphi_0 \in (0; \pi/2)$ let

$$E_{\varphi_0} := \{(a\cosh\vartheta\cos\varphi; a\sinh\vartheta\sin\varphi) : 0 \le \vartheta < \vartheta_0;\ |\varphi| < \varphi_0 \text{ or } |\pi - \varphi| < \varphi_0\}$$
$$= \{(x_1; x_2) \in E : |x_1| > a_1\cos\varphi_0\}.$$

Let

$$\eta_{\varphi_0}(m; n) := \left(\frac{\int_{E_{\varphi_0}} (u_{m;n})^2\,dx}{\int_E (u_{m;n})^2\,dx}\right)^{1/2}.$$

Our particular interest in this appendix is in families of eigenfunctions that are exponentially localised around the periodic orbit $\{(0; x_2) : |x_2| \le a_2\}$. In particular we will show below that the family $u_{m;0}$, $m = 0; 1; \ldots$ is so localised; precisely, we will show that, for all $\varphi_0 \in (0; \pi/2)$, there exists $\gamma > 0$ such that $\eta_{\varphi_0}(m; 0) = O(e^{-\gamma k_m})$ as $m \to \infty$.

Noting (A.5), we see that

$$\int_{E_{\varphi_0}} (u_{m;n})^2\,dx = 4a^2 \int_0^{\varphi_0}\int_0^{\vartheta_0} (\sinh^2\vartheta + \sin^2\varphi)\left[\mathrm{Mc}_n^{(1)}(\vartheta; q_{m;n})\mathrm{ce}_n(\varphi; q_{m;n})\right]^2 d\vartheta\,d\varphi.$$

Thus, defining

$$M_j := \int_0^{\vartheta_0} (\sinh\vartheta)^{2j}\left[\mathrm{Mc}_n^{(1)}(\vartheta; q_{m;n})\right]^2 d\vartheta; \quad I_s(m; n) := \int_0^{s} (\mathrm{ce}_n(\varphi; q_{m;n}))^2\,d\varphi;$$

it holds that

$$(\eta_{\varphi_0}(m; n))^2 \le \frac{(M_1 + M_0\sin^2\varphi_0)I_{\varphi_0}(m; n)}{M_1 I_{\pi/2}(m; n) + M_0\sin^2\varphi_0(I_{\pi/2}(m; n) - I_{\varphi_0}(m; n))} \cdot \frac{I_{\varphi_0}(m; n)}{I_{\pi/2}(m; n) - I_{\varphi_0}(m; n)}. \tag{A.8}$$

It is sufficient for the needs of this paper to estimate the asymptotics as $m \to \infty$ of $\rho_0(m;n)$ for $n = 0$, and so we will restrict our attention to this case. For this purpose, and abbreviating $q_{m;0}$ as q_m and $k_{m;0}$ as k_m, recall that $ce_0(\nu;q_m)$ satisfies (A.3) with $q = q_m$ and with $\lambda = a_0(q_m)$. Now the asymptotics of the eigenvalue $a_0(q)$ as $q \to \infty$ are known. From [14] we have that

$$a_0(q) = -2q + q^{1/2} + O(1) \tag{A.9}$$

as $q \to \infty$. Thus we see that, for

k

Since w'/w, $w''/w \in BC(\mathbb{R})$, the bilinear form a is bounded. For $\phi \in H^1(\mathbb{R})$,

$$a(\phi,\phi) = \int_{-1}^{1} \left((\phi')^2 + \frac{w'}{w}(\phi^2)' - p + 2\left(\frac{w'}{w}\right)^2 - \frac{w''}{w}\right)\phi^2 \, ds$$
$$= \int_{-1}^{1} \left((\phi')^2 - p + \left(\frac{w'}{w}\right)^2 \right)\phi^2 \, ds;$$

where the last step follows by integration by parts, on noting that $(w'/w)' = w''/w - (w'/w)^2$. Since $-p - (w'/w)^2 \geq c^2 - \gamma^{-2}$, a is coercive if $\gamma < c$, with

$$a(\phi,\phi) \geq \|\phi\|_1^2, \text{ where } \|\phi\|_1 := \left(\int_{-1}^{1} (\phi')^2 + (c^2 - \gamma^{-2})\phi^2 \, ds \right)^{1/2}.$$

Applying the Lax-Milgram lemma, it follows from (A.11) that

$$\sqrt{c^2 - \gamma^{-2}}\|v\| \leq$$

and choosing $\bar{} = c^2(o_c \ i \ o_0)=(1 + \sqrt{1 + (o_c \ i \ o_0)^2c^2}$